Wear 530-531 (2023) 205025

Contents lists available at ScienceDirect

Wear

journal homepage: www.elsevier.com/locate/wear

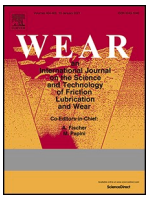

Effect of the addition of coated SiO_2 nanoparticles on the tribological behavior of a low-viscosity polyalphaolefin base oil

Fátima Mariño [a], José M. Liñeira del Río [a,b], David E.P. Gonçalves [b], Jorge H.O. Seabra [c], Enriqueta R. López [a], Josefa Fernández [a,*]

[a] Laboratory of Thermophysical and Tribological Properties, Nafomat Group, Department of Applied Physics, Faculty of Physics and Institute of Materials (iMATUS), Universidade de Santiago de Compostela, 15782, Santiago de Compostela, Spain
[b] Unidade de tribologia, vibraçoes e manutençao industrial, INEGI, Universidade do Porto, Porto, Portugal
[c] FEUP, Facultade de Engenharia da Universidade do Porto, Rua Dr. Roberto Frías s/n, 4200-465, Porto, Portugal

ARTICLE INFO

Keywords:
Low-viscosity oil
Nanoadditives
Anti-wear additives
Surface modification of NPs
Electric vehicles
Automatic transmission fluids

ABSTRACT

This work reports tribological properties of PAO6 containing SiO_2 nanoparticles modified with stearic-acid (SiO_2-SA) as additives at concentrations (0.05, 0.10, 0.20, 0.30) wt% and the same concentration of SA as a dispersant. Tribological experiments were performed at 120 °C in pure sliding and rolling-sliding conditions (5% slide-to-roll ratio). All nanolubricants have better anti-friction capabilities than PAO6. The optimum concentration for friction reduction was 0.30 wt% for both tribological conditions. The best anti-wear results for the specimens tested in pure sliding conditions were achieved with PAO6 + 0.20 wt% SiO_2-SA with reductions of 55%, 86% and 92%, in wear track width, wear track depth and wear area, respectively. Tribological mechanisms of the nanoparticles have been analyzed through roughness measurements, concluding that polishing, tribofilm and adsorption of the additives occur.

1. Introduction

Electric vehicles (EVs) are gaining relevance in recent years to reduce fuel consumption and air pollution. To further increase this positive outcome, it is important to enhance their performance. One way to improve the EV efficiency is to optimize the tribological behavior of the mechanical parts, such as the power transmission. For some configurations of EVs, transmission fluids must fulfill different requirements to those formulated for combustion vehicles. For the configurations where the electric engine and the transmission are in the same housing, the electric transmission fluids (ETF) should a) have ability to limit corrosion of copper and be compatible with polymers used in of the housing and in the electronic components; b) have low viscosity; c) show adequate electric properties [1–4]. The reason for using low viscosity lubricants is due to the high torque and operational speeds of tribological elements in EVs. By reducing the viscosity of the oil, viscous drag and viscous heating decrease and heat transfer is increased [5–7]. However, reducing the lubricant viscosity leads to a shift from full film to boundary lubrication, which can lead to severe surface contact and wear, which means that improved anti-wear and anti-friction properties are needed. One of the most successful methods to reduce friction and wear is the use of nanoadditives in lubricants [8,9]; which leads to a reduction in energy losses as well as emissions of pollutants, protecting the environment, and improves the life of machine elements [10–12]. An important factor in attaining a good nanolubricant is its stability for a prolonged period of time, the agglomeration of the nanoparticles (NPs) may lead to additive loss, efficiency reduction and machinery damage due to abrasive wear [9]. Several methods can be applied to enhance stability, such as physical treatment, use of surfactants and surface modification [13,14]. The need for more stable nanodispersions is especially relevant for those with lower viscosities due to the lower stability of the NPs in these fluids.

In addition to high torque and high speeds, the ETFs for EVs should endure high temperatures. Polyalphaolefins are broadly used in different applications due to the great capacity as lubricants and their oxidative and thermal stability, leading to better results compared to mineral oils [15]. In this work, polyalphaolefin 6 (PAO6) has been chosen owing to meet those characteristics as well as its low viscosity. Concerning PAO nanolubricants, some authors prepared dispersions with PAO6, which only have enough stability time to do the tribological

* Corresponding author.
E-mail address: josefa.fernandez@usc.es (J. Fernández).

https://doi.org/10.1016/j.wear.2023.205025
Received 13 April 2023; Received in revised form 12 June 2023; Accepted 14 June 2023
Available online 22 June 2023
0043-1648/© 2023 The Authors. Published by Elsevier B.V. This is an open access article under the CC BY-NC-ND license (http://creativecommons.org/licenses/by-nc-nd/4.0/).

measurements [16–18]. Ali et al. [19] solved this issue using oleic acid as a dispersant in a PAO (54 cSt at 40 °C) with Al_2O_3, TiO_2 or a combination of both NPs as nanoadditives remaining the nanodispersions stable for at least 35 days.

As regards the nanoadditives chosen in this work, silicon oxide NPs (SiO_2 NPs) have unique physical, chemical, and optical properties, so they can be applied in many fields [20]. These NPs have been analyzed as lubricant additives, showing great capability as friction and wear modifiers [21–25]. Cortés et al. [21] analyzed the effectiveness of uncoated spherical SiO_2 NPs (diameter 20–30 nm) as additives for a vegetable oil, obtaining reductions up to 77% for friction and 74% for wear volume. Zawawi et al. [26] used both SiO_2 NPs (30 nm) and Al_2O_3 NPs (13 nm) to prepare nanolubricants based on a PAG finding an optimum composite volume concentration of 0.02% at which the friction and wear rate reductions are 4.8% and 13%, respectively. Several authors [22–25,27] modified the surface of SiO_2 NPs to improve the stability of their nanodispersions, being a common modification their functionalization with oleic acid as was done by Peng et al. [22] achieving a stability time of around 30 days for a paraffin oil (43 cSt at 40 °C) with concentrations varying from 0.05 to 1.0 wt% of oleic acid modified SiO_2 NPs (92–110 nm). Peng et al. [23] also studied the influence of the size of SiO_2 NPs on tribological properties concluding that nanodispersions of the smallest oleic acid modified SiO_2 NPs (58 nm) in a paraffin oil showed the best tribological results and a stability of at least 30 days. Singh et al. [27] modified the surface of SiO_2 NPs (35 nm) with isopropyl alcohol and prepared nanodispersions of the modified NPs in epoxidized Madhuca indica oil (45.1 cSt at 40 °C) achieving strong friction and wear reductions with the nanodispersions of 0.8 wt% modified SiO_2 NPs. Silanization of SiO_2 NPs is another common surface-modification. Sui et al. [24] prepared hairy silica NPs (HSNs) with different ratios of two tethered silanes one polar and the other nonpolar, the more nonpolar tethered silane leads to the best stability time (2 months) due to the lower polarity of the resulting modified surface, which is more compatible with PAO100. Sui et al. [25] further confirmed the improvement of stability of HSNs with a nonpolar modification by comparing the effect of different tethered functionalities in amino silane modified SiO_2 NPs, the best stability results (2 months) in PAO100 were obtained for CH_3 terminated HSNs.

In this article, commercial SiO_2 NPs (8 nm) were chemically modified through stearic acid (SA) to improve its stability in PAO6. Several nanodispersions were tribologically tested using pure sliding conditions and rolling-sliding conditions (5% slide-to-roll ratio) at high temperature (120 °C). The worn surface in pure sliding condition tests was examined using a 3D optical profilometer and confocal Raman microscopy to understand the NPs tribological performance. For comparative reasons, the tribological effects of SiO_2-SA NPs were compared with those of a zinc dithiophosphate (ZDDP) and uncoated SiO_2 NPs. ZDDP is one of the most currently used friction and wear modifier additives in engine, industrial and transmission oils but for environmental restrictions and operational problems this additive should be replaced [28–30].

2. Experimental section

2.1. Materials and reagents

SiO_2 NPs (8 nm, 99%) were acquired from US Research Nanomaterials, Inc. (Houston, TX, USA). The reagents used in the esterification reaction were sodium hydroxide (0.05 M) from Honeywell (Charlotte, NC, USA), stearic acid (95%) from Sigma-Aldrich (Saint Louis, MO, USA) and hydrochloric acid (37%) from Merck (Darmstadt, Germany). The solvent used to transfer the NPs to PAO6 is n-hexane (95%) from Labkem (Barcelona, Spain). All these products were used with no additional purification. ZDDP was provided by REPSOL.

Polyalphaolefin base oil, PAO6, was provided by Repsol and has the following thermophysical properties: a density of 0.8114 g cm^{-3} and a kinematic viscosity of 30.62 cSt, both at 40 °C, as well as a viscosity index of 138. PAO6 oil was characterized by means of Fourier Transform Infrared Spectrometry (FTIR) and by Raman spectroscopy (Supplementary information, Figs. S1 and S2, respectively).

2.2. Stearic acid functionalization of SiO_2

An esterification reaction was used to functionalize the SiO_2 NPs with SA (Fig. 1), following a procedure similar to that of Mariño et al. [31]. Thus, commercial SiO_2 NPs (200 mg) were dispersed in distilled water (20 mL) in a round-bottom flask, containing a magnetic stir bar, and heated to 60 °C with 350 rpm agitation, using a magnetic hot-plate (Fig. 1a). Meanwhile, SA (415 mg) was dissolved in distilled water (10 mL) with the aid of ultrasonication (Fisherbrand Ultrasonic Bath, 180 W, 37 kHz). Once the SiO_2 aqueous dispersion reached the set temperature (60 °C), 5 mL of NaOH (0.05 M) were added (Fig. 1b). A minute later, the SA aqueous solution was added dropwise. The obtained mixture was kept for 30 min at 60 °C, and then refluxed at 95 °C for 90 min, finally obtaining the SA coated SiO_2 NPs (SiO_2-SA) dispersed in water (Fig. 1c).

The chemical composition of the SiO_2 NPs was analyzed by FTIR with a Nexus Thermo Nicolet spectrometer, using the attenuated total reflectance configuration (4000–400 cm^{-1}) and by a confocal Raman microscope (WITec Alpha300R+) with a 532 nm laser processing the data with the WITec Project FIVE software. The SA and SiO_2-SA NPs were also analyzed using FTIR and Raman to compare their spectra with those of uncoated NPs to confirm that the esterification reaction was carried out successfully.

2.3. Preparation and characterization of the nanodispersions

The dispersion method of the NPs in PAO6 is summarized in Fig. 2. After the esterification reaction, the aqueous nanodispersion was neutralized with HCl (37%), followed by a washing step using a MPW M-Universal Centrifuge (4000 rpm, 15 min): firstly, with distilled water, then with ethanol and finally with hexane. The collected NPs were redispersed in n-hexane for storage and subsequent handling. The reason for this washing step is to separate the SiO_2-SA NPs from the excess of SA and reaction impurities (such as NaCl) remaining in the water. After this purification process, the concentration of SiO_2-SA NPs was obtained by difference in weight of 1 mL of the nanodispersion before and after the evaporation of n-hexane. Then, a known amount of n-hexane nanodispersion was added to a given amount of PAO6. This new dispersion was homogenized by ultrasonication for 15 min and, after that, heated up to 95 °C, remaining at this temperature for 60 min to remove the n-hexane, obtaining a 4.7 wt% SiO_2-SA + PAO6 nanodispersion. Finally, this dispersion was diluted to obtain nanodispersions with concentrations of 0.3, 0.2, 0.1 and 0.05 wt% in SiO_2-SA. In order to further enhance the stability time of these last nanodispersions, the same wt% of SA as of SiO_2-SA was added as surfactant.

Furthermore, viscosity of the base oil and the formulated nanolubricants were measured at 0.1 MPa from 5 to 100 °C using a rotational viscosimeter Stabinger SVM3000 (Anton Paar, Graz, Austria). Experimental values of viscosity are presented in the supplementary information (Table S1). More details about the Stabinger SVM3000 were previously reported [31,32].

2.4. Tribological methods

Pure sliding tribological analyses with PAO6 and the SiO_2-SA + SA nanodispersions were performed with an Anton Paar MCR 302 modular rheometer equipped with a tribology cell T-PTD200 unit working in the rotational ball-on-three-pins configuration. Temperature was precisely monitored with a Peltier hood HPTD200. More details on configuration, characteristics, and experimental conditions of these experiments can be found in Table 1 and reference [32]. Furthermore, the same tests conditions were used for PAO6 + 0.2 wt% SA, PAO6 + 0.2 wt% SiO_2 NPs,

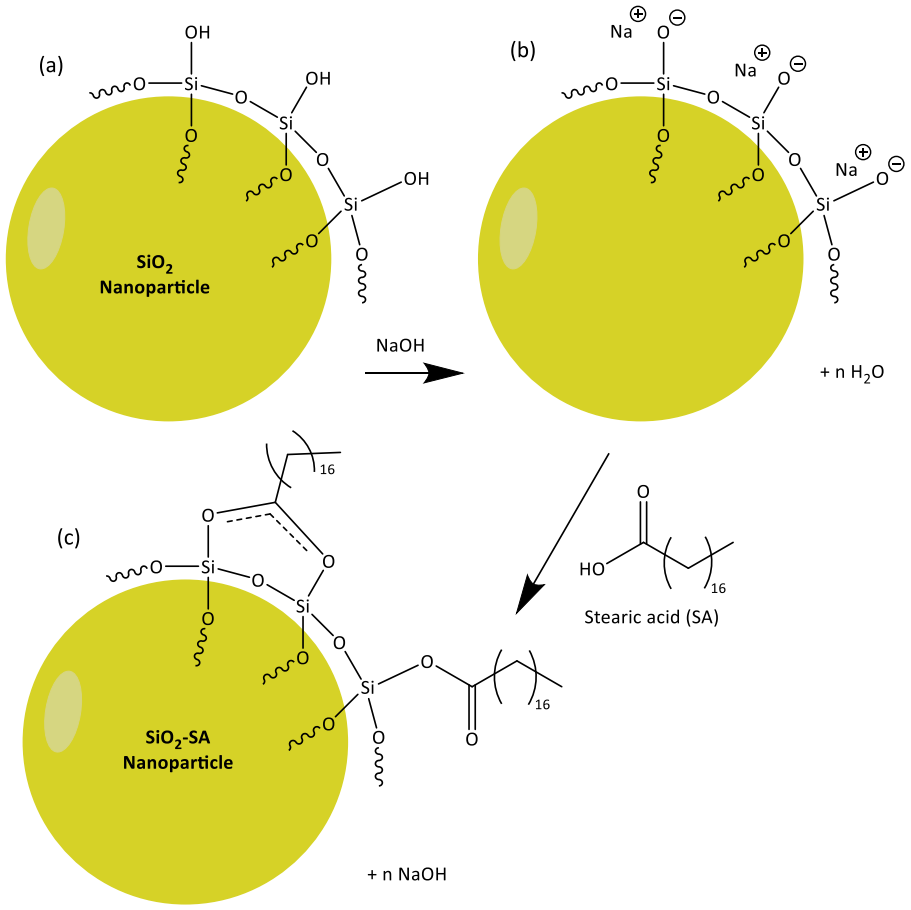

Fig. 1. Schematic drawing of the esterification reaction: a) SiO_2 NPs in water, b) after the addition of NaOH and c) after the SA addition.

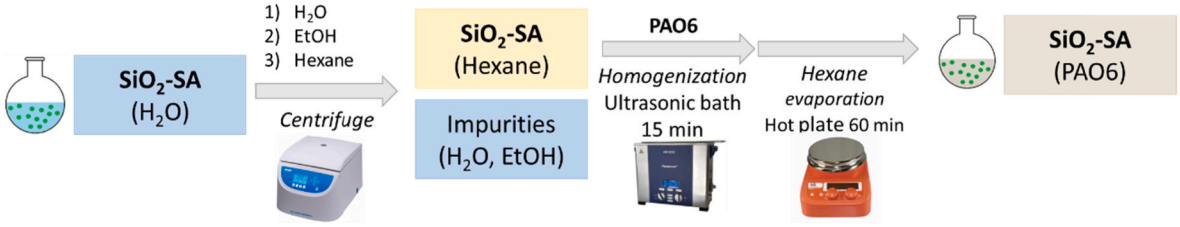

Fig. 2. Scheme of the dispersion method.

Table 1
Pure sliding tests: configuration of the tribometer, specimen details, and test conditions.

Tribology Cell T-PTD200 (Anton Paar)		
Ball-on-three pins configuration		Peltier hood HPTD200
Tribo-pair	Experimental conditions	
100Cr6 steel ball: 12.7 mm diameter and 0.15 μm Ra *100Cr6 pins:* 3 mm radius and a 0.3 μm Ra *Both:* Hardness: 58–65 HRC Young modulus: 190–210 GPa Poisson ratio: 0.29	Sample: 0.5 mL (3 replicates) Axial force (F): 20 N Tribological normal force (F_N): 9.43 N Maximum Hertzian contact pressure: 1.1 GPa Sliding distance: 340 m Rotational speed: 213 rpm Sliding speed: 0.10 m/s	120 °C

PAO6 + 0.2 wt% SiO_2-SA NPs and PAO6 + 0.2 wt% ZDDP. During each test, the values of the coefficient of friction, CoF, were recorded against the sliding distances, and their mean CoF value was determined. For each lubricant, the tests were repeated at least three times. Thus, from the mean CoF values of the repetitions, the average CoF value for each lubricant was determined and its standard deviation was calculated.

Table 2
Profilometer specifications and measured wear parameters.

S Neox (Sensofar)	
Specifications	Measured parameters
Mode: confocal Magnification objective: 10 × Software: SensoScan and SensoMap	Wear Track Width (WTW) Wear Track Depth (WTD) Worn area (Area) Surface roughness (Ra): • ISO 4287 standard • Gaussian filter wavelength cut-off: 0.025 mm

Prior to the wear analysis, the worn surface of the pins and the balls was cleaned with hexane. Subsequently, the wear-track on each pin and on the ball was characterized through a non-contact 3D optical profilometer (Sensofar S Neox), whose specifications are summarized in Table 2. The average values of these parameters and their standard deviations were obtained from the worn track profiles of the nine pins tested with each lubricant. To examine the effect of the presence of the NPs in the tribo-contact, the composition of the tribofilm formed in the worn pin surfaces was analyzed by confocal Raman microscopy (WITec Alpha300R+). To further analyze the effect of the additives in the worn pin surfaces, SEM micrographs of the PAO6 base oil and its formulated lubricants (PAO6 + 0.2 wt% SA, PAO6 + 0.2 wt% SiO_2 NPs PAO6 + 0.2 wt% SiO_2-SA NPs + 0.2 wt% SA, PAO6 + 0.2 wt% SiO_2-SA NPs and PAO6 + 0.2 wt% ZDDP) were obtained with a Zeiss Ultraplus Field Emission Scanning Electron Microscope, FESEM, at three magnifications (500x, 1000x and 2000x).

Moreover, rolling-sliding tribological tests were also carried out to measure the friction coefficient in different lubrication regimes using an EHD2 ball-on-disc test rig. The configuration of this apparatus consists of a rotating steel ball in contact with a rotating steel disc in rolling-sliding arrangement. The friction coefficient is measured with a torque cell coupled to a rotating ball shaft. Three steel discs with different roughness were used to cover the different lubrication regimes. The specimens and experimental conditions are presented in Table 3. The friction coefficient is determined from the friction force measured in negative and positive slide-to-roll ratio, SRR, (ball rotating faster than the disc and vice versa). The friction coefficient is obtained as the average of those achieved from two different friction tests: one ramp raising speed and the other one reducing speed. Additional information about this device was presented in an earlier article [33].

3. Results and discussion

3.1. Nanoparticle characterization

A JEOL JEM-1011 Transmission Electron Microscope (TEM) was used to observe the morphology of the uncoated SiO_2 nanopowders. TEM images (Fig. 3) of the nanopowders, dispersed previously in water, show small agglomerates of roughly spherical NPs.

The infrared spectra of pure SA, commercial SiO_2 NPs and dried SiO_2-SA NPs are displayed in Fig. 4. Table 4 shows details of the characteristic peaks of these spectra. The FT-IR spectrum of SiO_2-SA NPs shows signals from both SiO_2 NPs and SA, which are: two symmetrical stretching bands at 2917 and 2848 cm^{-1} corresponding to C–H bond in $–CH_3$ and $–CH_2$ from the SA, as well as two wagging vibration bands at 1458 and 1450 cm^{-1} of C–C in $–CH_2$ [34]; some important weaker peaks appear at 1683 and 1064 cm^{-1}, the former due to the C═O stretching of the SA and the later from the Si–O–Si anti-symmetric stretching of the SiO_2 NPs [35]. All these signals present a slight shift compared to those of SA and SiO_2 counterparts, most likely due to the strong interactions between both core and shell. An important evidence for the existence of covalent bonds between them is the absence of FT-IR signals corresponding to in-plane and out-of-plane bending O–H vibrations [36] at 1429 and 939 cm^{-1} respectively, which appear in the FT-IR spectrum of SA. Furthermore, the drop in the intensity of the C═O stretching band shows that some of the SA molecules have reacted with both types of oxygen atoms, –OH and C═O, as it has been represented in Fig. 1. To further study the composition of SiO_2 NPs, SA dispersant, and SiO_2-SA NPs, a Raman analysis was performed (Supplementary information, Fig. S2), whose Raman spectrum was also used in section 3.3 for the Raman analysis of the worn surface.

Table 3
Rolling-sliding tribometer: specimen characteristics and experimental conditions.

EHD2 apparatus (PCS Instruments)		
Disc and Ball Specimens	Experimental conditions	
Material: 100Cr6 steel	Temperature:	120 °C
Young modulus: 210 GPa	Load:	50 N
Poisson ratio: 0.29	SRR:	5%
Disc diameter: 100 mm	Speed:	Ramp from 0.05 to 2 m s^{-1}
Ball diameter: 19.05 mm	Sample:	120 mL
Surface roughness		
smooth disc, Ra = 0.02 μm		
rough disc 1, Ra = 0.10 μm		
rough disc 2, Ra = 0.34 μm		
ball, Ra = 0.02 μm.		

3.2. Nanolubricant stability

The stability of the nanodispersions was assessed by visual observation over time until sedimentation was detected. The images are shown in Fig. 5. Just after their preparation, the SiO_2 and SiO_2-SA + SA nanodispersions presented a high transparency (Fig. 5a and d). The nanodispersion with uncoated NPs sedimented after 24 h. Thus, a yellow-white turbidity appeared in the bottom of the flask (Fig. 5b), turning more yellow and compact over time (Fig. 5c). In contrast, the SiO_2-SA nanodispersion kept the same slightly white and transparent appearance even after 100 days (Fig. 5f). Therefore, the nanodispersion containing the SA-modified SiO_2 NPs showed an important enhancement of the stability compared to that containing unmodified SiO_2 NPs.

3.3. Tribological results

3.3.1. Pure sliding conditions

Table 5 and Fig. 6 summarize the average CoF values for PAO6 and for the studied lubricants. All the nanodispersions (PAO6 + SiO_2-SA NPs + SA) lead to coefficients of friction lower than the ones measured for the PAO6 base oil, the reductions varying from 15 to 56%, depending on the concentration. The mass concentrations of the dispersions leading to the most significant CoF reductions are (0.2 and 0.3) wt% SiO_2-SA NPs + (0.2 or 0.3) wt% SA in PAO6. Comparing the coefficients of friction of the PAO6 + 0.2 wt% SiO_2-SA NPs + 0.2 wt% SA nanodispersions with that of PAO6 + 0.2 wt% SA mixture, the former showed a 17% coefficient of CoF reduction compared to the latter. SA and SiO_2-SA NPs seem to have a synergistic effect: the reduction of CoF of the combined additives (53%) is higher than the reductions of friction obtained when only one of the additives is present, the PAO6 + SA mixture shows a 44% reduction and the PAO6 + SiO_2-SA NPs nanodispersion a 15% reduction, both compared to the base oil. In addition, the SA coating on the SiO_2 NPs surfaces leads to a higher CoF reduction than uncoated SiO_2 NPs, which did not have any CoF reduction effect on the PAO6 base oil. Besides, the PAO6 + 0.2 wt% SiO_2-SA NPs + 0.2 wt% SA nanodispersion has shown higher coefficient of friction reduction than that of PAO6 + 0.2 wt% ZDDP mixture, which had a 33% reduction compared to PAO6.

The wear of the worn surfaces of the pins tested in the friction tests was analyzed using a 3D profilometer. Table 6 summarizes the average values of the Wear Track Width (WTW), Wear Track Depth (WTD) and worn area (area) and the expanded uncertainties, U (k=2). The WTD values are plotted in Fig. 6 for the studied lubricants. All the nanodispersions (SiO_2-SA + SA) lead to lower WTD values than PAO6. In what regards to wear, the optimum nanolubricant leading to the highest reductions for all the wear parameters (55%, WTW; 86%, WTD; and 92% worn area) is the PAO6 + 0.20 wt% SiO_2-SA + 0.20 wt% SA nanodispersion.

In Fig. 7 the profiles of the worn surfaces obtained with PAO6 and each nanodispersion (PAO6 + SiO_2-SA NPs + SA) are shown. The largest groove is obtained using the base oil, and the narrowest one using PAO6 + 0.20 wt% SiO_2-SA NPs + 0.20 wt% SA nanodispersion. Comparing the PAO6 + 0.20 wt% SiO_2-SA NPs + 0.20 wt% SA nanodispersion with the PAO6 + 0.20 wt% SA mixture, the former showed an 86% reduction in WTD compared to the latter, which only led to a wear reduction of 3% in

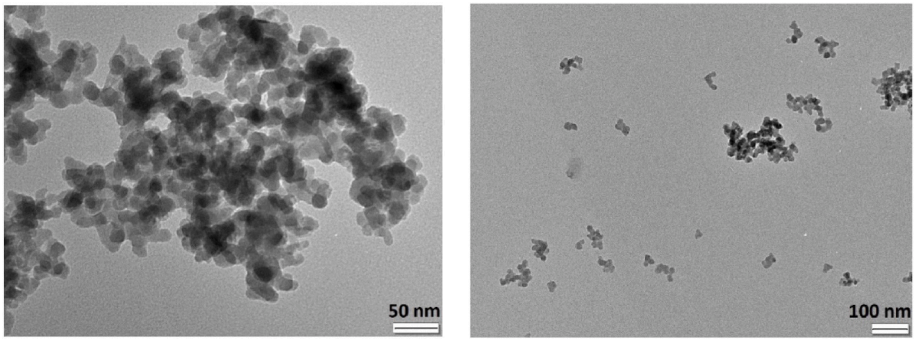

Fig. 3. TEM micrographs of the uncoated SiO_2 NPs.

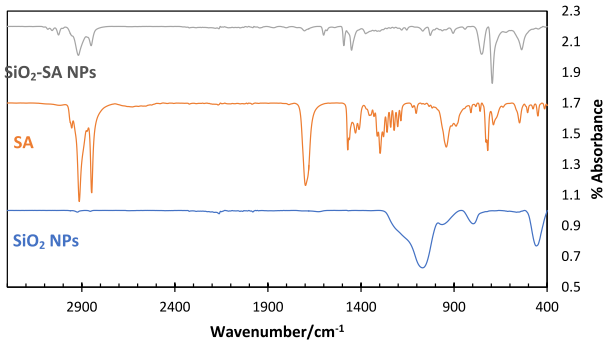

Fig. 4. FTIR spectra of uncoated SiO_2 NPs (blue), SA (orange) and SiO_2-SA NPs (grey). (For interpretation of the references to color in this figure legend, the reader is referred to the Web version of this article.)

Table 4
FTIR spectra: wavenumber and vibration mode assigned to each chemical bond.

Substance	Peak (cm^{-1})	Vibration mode		Chemical bond
SiO_2	1064	ν_{as}	Anti-symmetric stretching	Si–O–Si
	950	ν	Stretching	Si–O
	782	δ	Bending	Si–O–Si
	451	ρ	Rocking	Si–O
SA	2913	ν_s	Symmetrical stretching	C–H bond in $–CH_3$
	2846	ν_s	Symmetrical stretching	C–H bond in $–CH_2$
	1700	ν	Stretching	C═O
	1429	δ_{ip}	In-plane bending	O–H
	1400–1180	ω	Wagging	C–C in $–CH_2$
	939	δ_{oop}	Out-of-plane bending	O–H
SiO_2-SA	2917	ν_s	Symmetrical stretching	C–H bond in $–CH_3$
	2848	ν_s	Symmetrical stretching	C–H bond in $–CH_2$
	1683	ν	Stretching	C═O
	1454	ω	Wagging	C–C in $–CH_2$
	1450	ω	Wagging	C–C in $–CH_2$
	1064	ν_{as}	Anti-symmetric stretching	Si–O–Si

WTD compared to PAO6. The reduction in WTD obtained with PAO6 + 0.20 wt% SiO_2-SA NPs was also lower (30%) than using combination of both additives (86%), which indicates a great synergy between both additives. This trend is similar to that obtained for the coefficient of friction results. Hence, the nanodispersion containing both SiO_2-SA NPs and SA showed an enhanced tribological behavior. Concerning the SA coating effect on the SiO_2 anti-wear results, the nanodispersion containing commercial SiO_2 NPs was the only one that worsen the PAO6

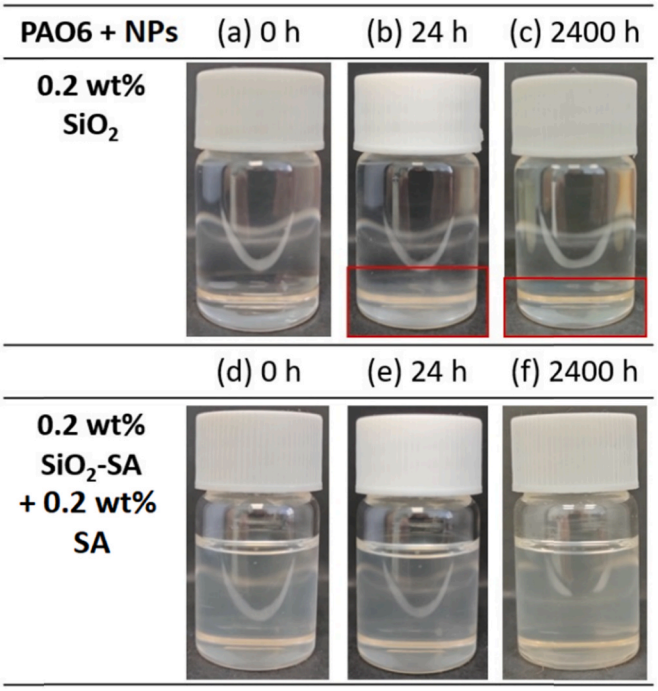

Fig. 5. Photographs of PAO6 + 0.2 wt% SiO_2 and PAO6 + 0.2 wt% SiO_2-SA + 0.2 wt% SA dispersions at 0 h (a,d), 24 h (b,e) and 2400 h (c,f) after their preparation.

Table 5
Average coefficients of friction, CoF, at 120 °C and the expanded uncertainties, U (k=2), for PAO6 base oil and all studied lubricants.

Lubricants	CoF	U	Reduction % compared to PAO6
PAO6	0.1542	0.0026	
0.05 wt% SiO_2-SA + 0.05% SA	0.1316	0.0021	15
0.10 wt% SiO_2-SA + 0.10% SA	0.1264	0.0014	18
0.20 wt% SiO_2-SA + 0.20% SA	0.0719	0.0015	53
0.30 wt% SiO_2-SA + 0.30% SA	0.0680	0.0003	56
0.2 wt% SA	0.0864	0.0048	44
0.2 wt% SiO_2	0.1554	0.0039	0
0.2 wt% SiO_2-SA	0.1303	0.0063	15
0.2 wt% ZDDP	0.1034	0.0022	33

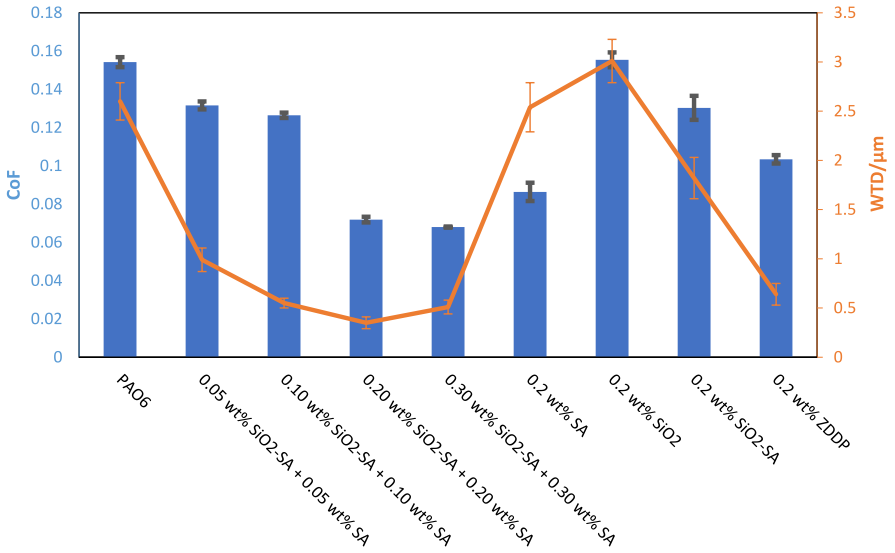

Fig. 6. Average coefficients of friction, CoF, (blue) and wear track depth, WTD, (orange) for PAO6 and PAO6 and the studied lubricants. (For interpretation of the references to color in this figure legend, the reader is referred to the Web version of this article.)

Table 6
Average values of the worn pin surface width, WTW, depth, WTD, and area of worn tracks and the expanded uncertainties, U (k=2), for PAO6 and all studied lubricants.

Lubricants	WTW/ µm	U/ µm	WTD/ µm	U/ µm	Area/ µm^2	U/ µm^2
PAO6	435	10	2.60	0.19	806	65
0.05 wt% SiO_2-SA + 0.05 wt% SA	256	14	0.99	0.12	200	32
0.10 wt% SiO_2-SA + 0.10 wt% SA	268	19	0.55	0.05	104	18
0.20 wt% SiO_2-SA + 0.20 wt% SA	195	17	0.35	0.06	40	9
0.30 wt% SiO_2-SA + 0.30 wt% SA	240	18	0.51	0.07	61	12
0.20 wt% SA	422	19	2.54	0.25	723	76
0.20 wt% SiO_2	471	21	3.01	0.22	967	69
0.20 wt% SiO_2-SA	342	14	1.82	0.21	353	44
0.20 wt% ZDDP	232	12	0.64	0.11	81.2	13

wear results, increasing a 15% the WTD compared with PAO6. Furthermore, the optimal nanodispersion of PAO6 + 0.20 wt% SiO_2-SA NPs + 0.20 wt% SA also has a better wear reduction capability compared to the PAO6 + 0.20 wt% ZDDP, which had a 75% WTD reduction compared to PAO6 base oil.

The arithmetic average roughness, Ra, was also measured through 3D profilometry, considering a gaussian filter 0.25 mm. This parameter is useful to identify the anti-wear mechanisms of NPs. In Table 7 the average values of Ra are plotted for all the worn surfaces lubricated with PAO6 and PAO6 + SiO_2-SA NPs + SA nanodispersions, as well as for the unworn surface of a pin. All the nanodispersions led to worn tracks with smaller Ra than those of the unworn surface and of the worn pins lubricated with PAO6. The lowest Ra is that of the worn surface lubricated with PAO6 + 0.3 wt% SiO_2-SA NPs being 41% lower than that of

Table 7
Average values of the Ra and Rq of untested pin surface, worn tracks and the expanded uncertainties, U (k=2), for PAO6 and PAO6 + wt% SiO_2-SA NPs + wt % SA nanodispersions.

	Ra/nm	U/nm	Rq/nm	U/nm
PAO6	11.2	1.4	15.3	2.4
0.05 wt% SiO_2-SA NPs+ 0.05 wt% SA	8.5	0.6	10.4	0.7
0.10 wt% SiO_2-SA NPs+ 0.10 wt% SA	6.1	1.0	8.8	2.5
0.20 wt% SiO_2-SA NPs+ 0.20 wt% SA	6.2	1.3	7.3	1.5
0.30 wt% SiO_2-SA NPs + 0.30 wt% SA	5.2	0.7	6.2	0.9
Untested Pin	8.9	0.6	10.4	0.6

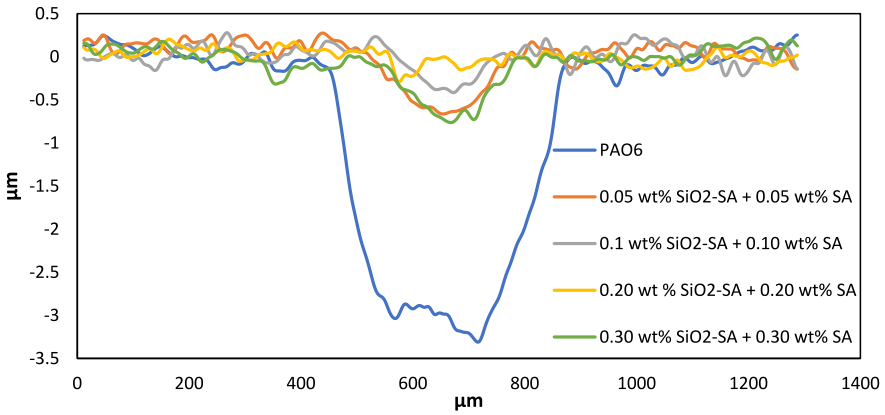

Fig. 7. Profile images of worn pin tracks lubricated with PAO6 (blue) and PAO6 + wt% SiO_2-SA + wt% SA nanodispersions (0.05 wt%, orange; 0.1 wt% grey; 0.2 wt %, yellow; 0.3 wt%, green). (For interpretation of the references to color in this figure legend, the reader is referred to the Web version of this article.)

the unworn surface, and 53% of the worn surface lubricated with PAO6. However, 0.1 and 0.2 wt% nanodispersions exhibit very similar results with more than a 30% reduction compared to the unworn surface and a 45% compared to the worn surface from PAO6.

Another parameter used to characterize the topology of the surfaces is the root mean square roughness (Rq), which is more sensitive to large deviation from the mean line than Ra [37]. The same trend with lubricants and pins for Ra and Rq have been found, as can be seen in Table 7.

3D images of the worn tracks of the steel balls used in the friction tests are shown in Fig. 8. The nanolubricant containing SiO_2-SA and SA as dispersant led to the lowest wear on the ball, 173 μm for WTW. Interestingly, the absence of SA dispersant (PAO6 + 0.20 wt% SiO_2 NPs and PAO6 + 0.20 wt% SiO_2-SA NPs) resulted in WTW values similar to or higher than that obtained with neat PAO6 base oil. However, the use of only SA as an additive generated a slightly higher WTW value (201 μm) compared to the optimal nanodispersion, which is coherent with the wear results of the pins, thus a synergistic effect of both additives is observed. The ball lubricated with PAO6 containing ZDDP as additive showed good wear reduction, although the WTW value was higher (199 μm) than that obtained for the optimal nanodispersion.

Furthermore, Raman mappings of the worn tracks of pins show distinctive areas corresponding to different compounds indicated with several colors (Figs. 9 and 10). For the assignation of the components in the worn surface, the Raman signals were separated using the software Project FIVE. Concerning the worn pins tested with the base oil (Fig. 9) the presence of PAO6 (blue), as well as of iron oxides (yellow) and of carbon (green) coming from the lubricant degradation were observed [31]. On the other hand, the Raman mapping from the 0.20 wt% SiO_2-SA NPs + 0.20 wt% SA nanodispersion in PAO6 (Fig. 10) indicates the presence of SiO_2 NPs (red), as well as of PAO6 (blue) and of carbon (green). The presence of SiO_2 NPs is confirmed by the appearance of an intense and sharp peak close to 500 cm^{-1} [38]. This peak does not appear in the Raman spectrum of iron oxide, which instead presents peaks of similar intensity in the lower region of the spectrum (Fig. 9) [39], i.e., with the addition of SiO_2-SA NPs, iron oxides were not observed. On the other hand, in the Raman spectra of the mapping of Fig. 10, the lack of SA signal (absence of C–H characteristic peaks around 3000 cm^{-1}) reveals that, during the tribo-tests, some tribo-chemical reactions occur promoted by the high both temperatures and pressures due to the friction process. Thus, these conditions cause the breaking of the bonds between SA and the coated SiO_2 NPs, similarly to what was found by Zhang et al. [40] for SA modified TiO_2 NPs through XPS. Assuming the same hypothesis as these authors [40], the uncoated SiO_2 NPs are easily adsorbed on the worn surface, generating a boundary lubricating film. Moreover, the SA could be physically adsorbed on the steel surface during the tribotests [41–43] and be removed with the hexane solvent in the cleaning process of the worn pins before the Confocal Raman Analysis.

In Figs. 9 and 10, the presence of the chemical components coincides with the direction of the grooves formed during the tribological experiments. In addition, there is a great presence of PAO6 in the worn pin tested with the base oil. When adding the SiO_2-SA NPs and SA to the PAO6 lubricant the tribofilm created in the worn track is mainly composed by SiO_2 NPs and carbon, being the tribological mechanisms governed by the nanoparticles rather than the base oil. Considering the roughness and these Raman results it can be assumed that on the worn surface tribofilm formation, and polishing and mending effects occur.

Regarding the SEM micrographs of the worn pins (Fig. 11), inspection of these images reveals that abrasive wear in the sliding direction is the main wear mechanism in the case of the PAO6-lubricated worn surface, with an evident ploughing even at the lowest magnification (500x). This type of wear is slightly reduced when SA is used as the only additive. The addition of SiO_2 or SiO_2-SA NPs reduce the grooves in the worn surface but microcracks appear on the surfaces. Furthermore, when ZDDP is used as PAO6 additive, although the wear track is greatly reduced, the surface shows similar damage. The least damaged surface is the one obtained using PAO6 + 0.20 wt% SiO_2-SA NPs + 0.20 wt% SA as lubricant, which once again highlights the positive synergies between both additives, which increase scuffing resistance and reduce wear. These results agree with those obtained with profilometry for the pins.

3.3.2. *Rolling-sliding conditions*

Rolling-sliding tribological results obtained with PAO6 base oil and the SiO_2-SA NPs + SA nanodispersions are presented as Stribeck curves (Figs. 12 and 13). For this aim, these curves are built by plotting the coefficient of friction against the specific lubricant film thickness, Λ, that was defined as:

$$\Lambda = h_c / Ra \quad (1)$$

where h_c corresponds to the theoretical central film thickness and Ra is the equivalent average surface roughness of the contacting surfaces, given by $Ra = \sqrt{(Ra_{disc}^2 + Ra_{ball}^2)}$. In this case, the lubricant central film thickness, h_c, at the operating temperature (120 °C) was predicted by means of the Hamrock and Downson's equation [44], taking into account different parameters related to the geometrical and mechanical properties of ball and discs, lubricant properties (viscosity and pressure−viscosity coefficient) and finally the test parameters like speed, load and SRR (slide-to-roll ratio).

For each tested lubricant, the experimental dynamic viscosity values from 5 °C to 100 °C (Table S1) were correlated through the

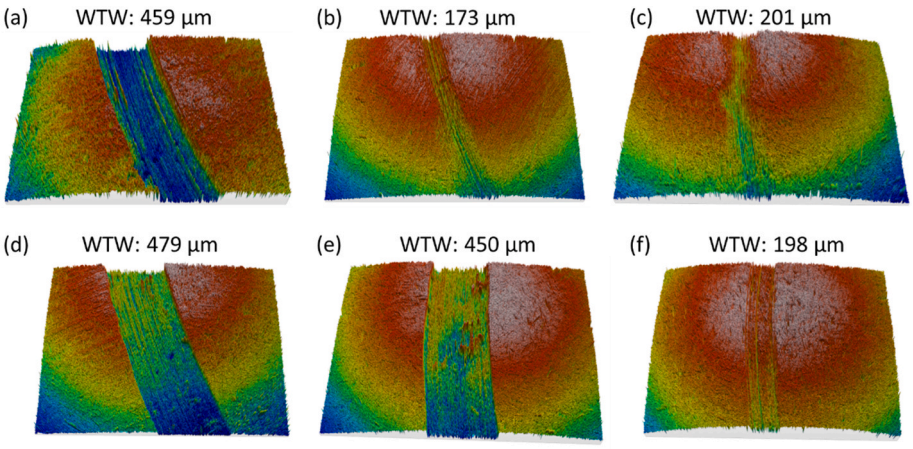

Fig. 8. 3D images of the worn ball surfaces for (a) PAO6, (b) PAO6 + 0.20 wt% SiO_2-SA NPs + 0.20 wt% SA, (c) PAO6 + 0.20 wt% SA, (d) PAO6 + 0.20 wt% SiO_2 NPs, (e) PAO6 + 0.20 wt% SiO_2-SA NPs, (f) PAO6 + 0.20 wt% ZDDP, and their WTW values.

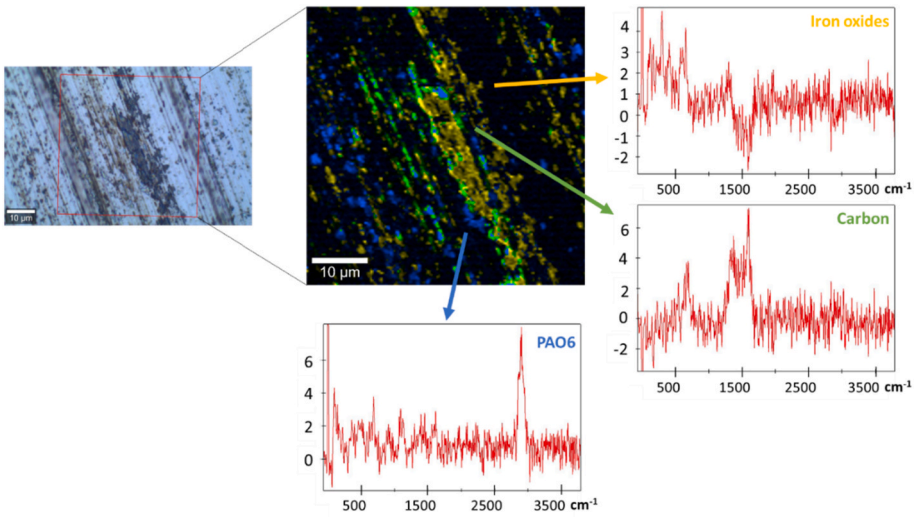

Fig. 9. Elemental mapping and Raman spectra of worn pins tested with PAO6 base oil.

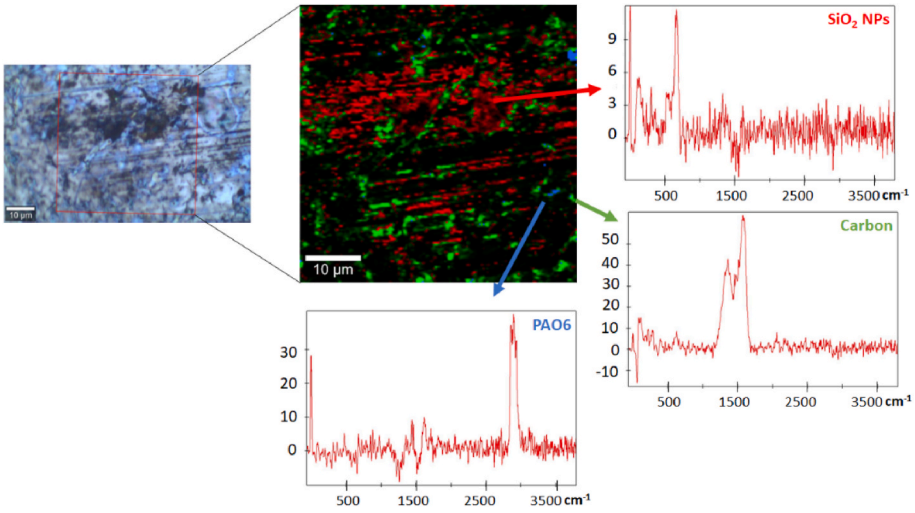

Fig. 10. Elemental mapping and Raman spectra of worn pins tested with PAO6 + 0.20 wt% SiO_2-SA NPs + 0.20 wt% SA nanolubricant.

Vogel−Fulcher−Tammann (VFT) equation. The dynamic viscosity of each nanolubricant and base oil at 120 °C and 0.1 MPa was obtained by extrapolation of the VFT correlations. This methodology was used because the Stabinger SVM3000 viscometer does not permit viscosity measurements above 100 °C. The pressure−viscosity coefficient of PAO6 was taken from Ref. [45]. Due to the low concentration of the NPs, for the three nanolubricants their pressure−viscosity coefficient values were considered equal to those of PAO6.

Fig. 12 shows the Stribeck curves for PAO6 neat oil as well as for SiO_2-SA nanolubricants using three different discs: smooth, rough 1 and rough 2 discs (see Table 3). As expected, ball-on-disc tests using the rough discs generate lower Λ values and consequently show higher coefficients of friction than those performed with the smooth disc. At the lowest specific lubricant film thickness, i.e., lowest entrainment speeds, the coefficient of friction values are much lower with any nanolubricants (SiO_2-SA + SA) than with the PAO6 neat oil, for all discs. Therefore, the key effect of SiO_2-SA nanoparticles is to significantly reduce the friction under boundary film when the lubricant film build-up is poor (low speeds and low Λ values).

Concerning the effect of mass concentration of nanoadditives in the tribological performance, the CoF decreases as the concentration of nanoadditives rises in the studied range. For this reason, the Stribeck curve of PAO6 neat oil together with that of 0.30 wt% SiO_2-SA + 0.30 wt % SA nanolubricant was plotted in Fig. 13. This result agrees with the coefficient of friction measurements achieved for the pure sliding tests, where the 0.30 wt% SiO_2-SA NPs + 0.30 wt% SA was one of the optimal concentrations as anti-friction nanolubricant. At high entrainment speeds (right section of the Stribeck curves) and therefore large specific lubricant film thickness, the coefficient of friction is quite similar for all nanolubricants and base oil.

Generally, under elastohydrodynamic (EHD) lubrication, a typical full Stribeck curve shows three lubrication regimes: boundary film, mixed film, and full film lubrication. In general, boundary film lubrication appears if $\Lambda < \Lambda_0$, mixed film lubrication if $\Lambda_0 \leq \Lambda \leq \Lambda_1$, and EHD lubrication if $\Lambda > \Lambda_1$ [46,47]. The values of Λ_0 and Λ_1, depend on several parameters, in particular the composite surface roughness, lubricant additives, lubricant temperature (120 °C) and the application (e.g., ball-on-disc geometry, rolling bearings, gears).

In Fig. 13 the coefficients of friction corresponding to PAO6 and to the nanodispersion (PAO6 + 0.30 wt% SiO_2-SA NPs + 0.30 wt% SA) are plotted against Λ defined by equation (1). In the case of the nanodispersion, it can be observed that for $\Lambda < 0.08$ (approximately) the coefficient of friction is almost constant (CoF ≈ 0.04) which is typical of the boundary film lubrication regime of lubricants containing additives.

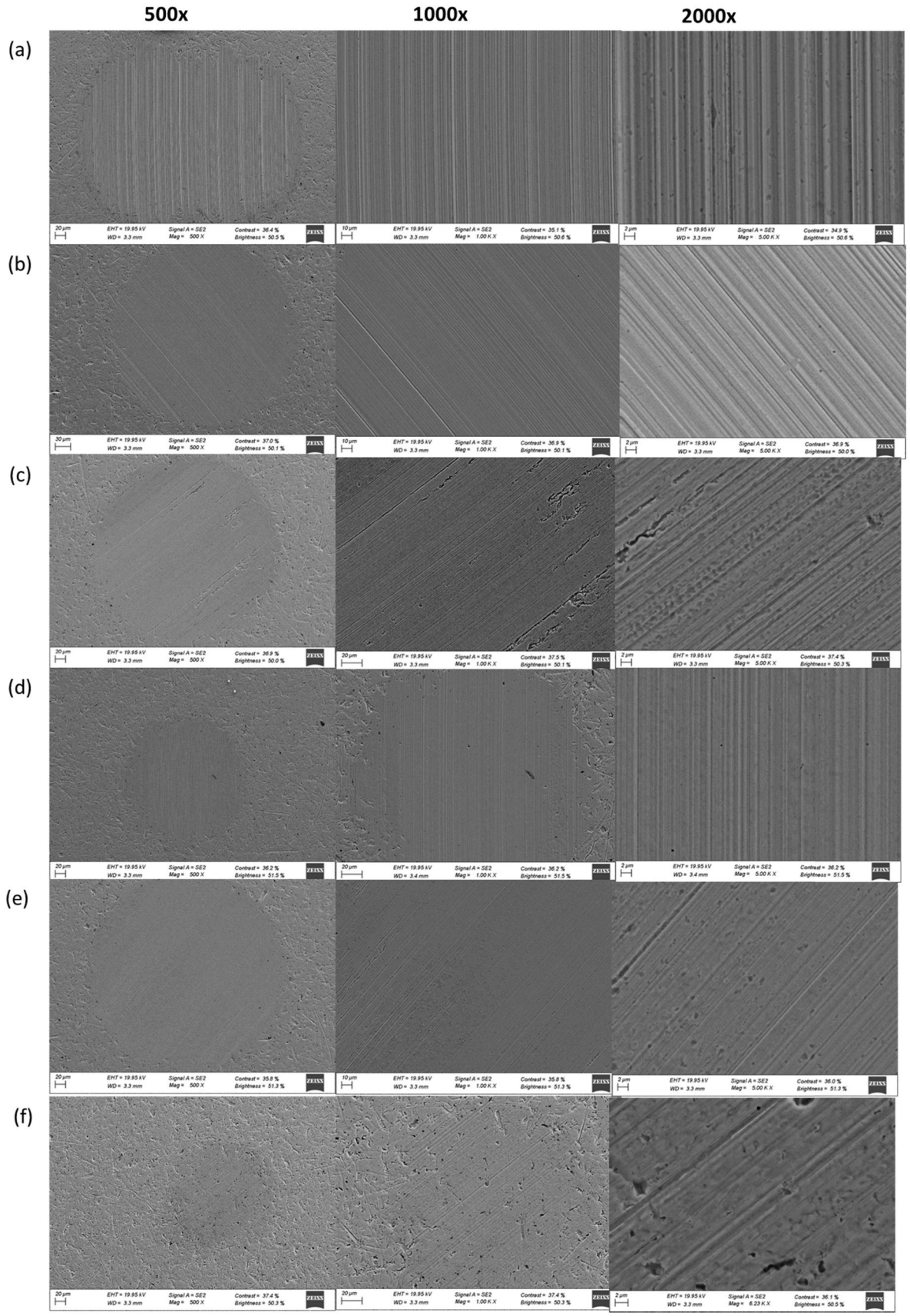

Fig. 11. SEM micrographs at three magnifications of the worn pin surfaces lubricated by (a) PAO6, (b) PAO6 + 0.20 wt% SiO_2-SA NPs + 0.20 wt% SA, (c) PAO6 + 0.20 wt% SA, (d) PAO6 + 0.20 wt% SiO_2 NPs, (e) PAO6 + 0.20 wt% SiO_2-SA NPs, (f) PAO6 + 0.20 wt% ZDDP.

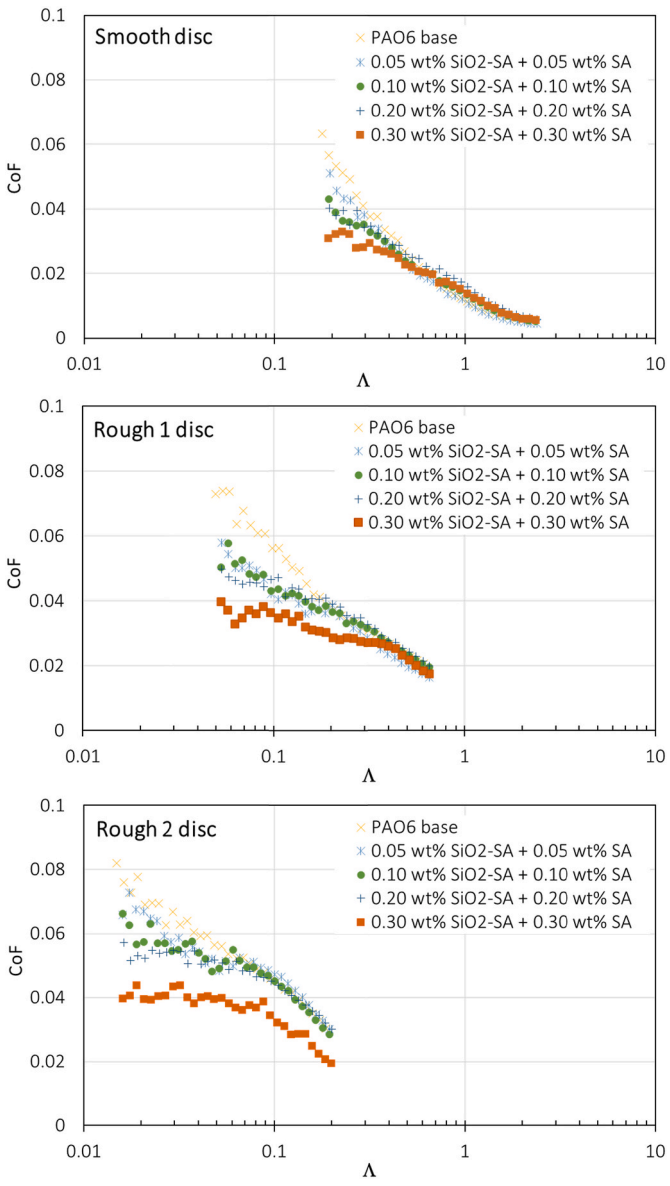

Fig. 12. Partial Stribeck curves of PAO6 and SiO_2-SA + SA nanodispersions tested for three different discs at 120 °C and 5% SRR.

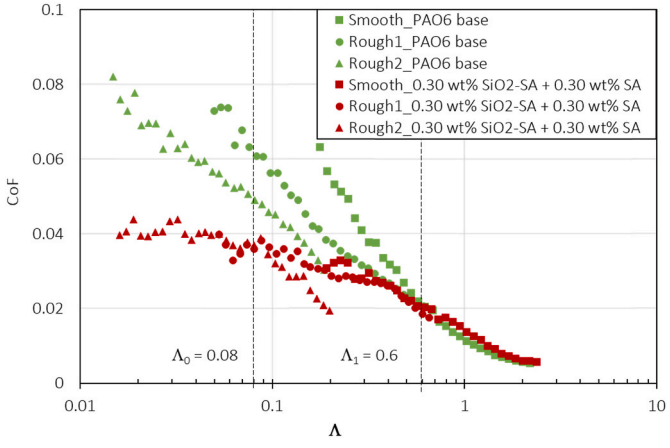

Fig. 13. Stribeck curves of PAO6 and 0.30 wt% SiO_2-SA + 0.30 wt% SA nanodispersions tested for the three discs at 120 °C and 5% SRR.

For $0.08 < \Lambda < 0.6$ (approximately) the CoF decreases as the Λ values increase, which is typical of the mixed film lubrication regime.

It is also clear that for $\Lambda < 0.6$ (within the boundary and mixed film regimes) there is a significant different behavior between the nanodispersion and the PAO6 base oil. In fact, in the case of the PAO6 base oil the coefficient of friction increases continuously as the Λ decreases, which is typical of base oils without additives.

For $\Lambda > 0.6$ the coefficient of friction decreases as Λ increases, but there are no significant differences between the nanodispersion and the PAO6 base oil, meaning that the influence of the nanoparticles (that is additives) and of the surface roughness are no longer significant, which is typical of full film lubrication regime.

The values of $\Lambda_0 \approx 0.08$ and $\Lambda_1 \approx 0.6$ observed in this case are not general, they fit the contact geometry considered (ball-on-disc), the roughness parameter (Ra) considered to define Λ and the test temperature (120 °C in the present case).

4. Conclusions

SiO_2 NPs were successfully coated with SA, greatly improving the stability of their PAO6 based nanodispersions compared with that of the nanodispersions containing uncoated SiO_2 NPs.

Improvements in friction and wear results have been obtained at 120 °C with reductions up to 56% for friction coefficient and up to 92% for wear area, respect to those obtained with PAO6, at pure sliding conditions. The NPs optimal concentrations are 0.2 and 0.3 wt% depending on the parameter evaluated; overall, the best concentration is 0.2 wt% due to the excellent reductions with less nanoparticle amount. There is a synergistic effect between the SiO_2-SA NPs and the SA dispersant, showing the combination of both additives the best reductions of friction and wear. In addition, the SA coating of NPs reduces friction and wear compared to the uncoated SiO_2 NPs. The wear results from the steel balls and the SEM micrographs from the pins agree with the wear results evaluated from the pins. The 0.20 wt% SiO_2-SA NPs + 0.20 wt% SA nanodispersion has proven to be an alternative to ZDDP. All the nanodispersions led to roughness reductions of the worn surfaces. This fact together with the presence of SiO_2 NPs in the worn surfaces shown through Raman microscopy (Fig. 10) lead to the conclusion that polishing, tribofilm and adsorption of the additives on the contact surface occur.

Significant reductions of the coefficient of friction were observed, not only under pure sliding conditions, but also in rolling-sliding conditions. As far as we know, this is the first time that strong friction reductions due the NPs were found under rolling-sliding conditions.

CRediT authorship contribution statement

Fátima Mariño: Writing – review & editing, Writing – original draft, Methodology, Investigation, Conceptualization. **José M. Liñeira del Río:** Writing – review & editing, Methodology, Investigation, Conceptualization. **David E.P. Gonçalves:** Writing – review & editing, Methodology, Validation, Supervision, Formal analysis. **Jorge H.O. Seabra:** Writing – review & editing, Project administration, Funding acquisition. **Enriqueta R. López:** Writing – review & editing, Validation, Supervision, Formal analysis. **Josefa Fernández:** Writing – review & editing, Validation, Supervision, Project administration, Funding acquisition, Conceptualization.

Declaration of competing interest

The authors declare that they have no known competing financial interests or personal relationships that could have appeared to influence the work reported in this paper.

Data availability

Data will be made available on request.

Acknowledgments

This research is supported by Xunta de Galicia (ED431C 2020/10), by MCIN/AEI/10.13039/501100011033 through the PID2020-112846RB-C22 project and by LAETA, Portugal, under project UID/50022/2020. JMLdR is grateful for financial support through the Margarita Salas program, funded by MCIN/AEI/10.13039/501100011033 and "NextGenerationEU/PRTR". FM acknowledges a IACOBUS grant to the European Grouping for Territorial Cooperation Galicia-North of Portugal (GNP-EGTC). Furthermore, authors are also grateful to Repsol Lubricants for providing the PAO6 base oil and to RIAIDT-USC for its analytical facilities.

Appendix A. Supplementary data

Supplementary data to this article can be found online at https://doi.org/10.1016/j.wear.2023.205025.

References

[1] L.I. Farfan-Cabrera, Tribology of electric vehicles: a review of critical components, current state and future improvement trends, Tribol. Int. 138 (2019) 473–486, https://doi.org/10.1016/j.triboint.2019.06.029.
[2] A. García Tuero, N. Rivera, E. Rodríguez, A. Fernández-González, J.L. Viesca, A. Hernández Battez, Influence of additives concentration on the electrical properties and the tribological behaviour of three automatic transmission fluids, Lubricants 10 (2022) 276, https://doi.org/10.3390/lubricants10110276.
[3] E. Rodríguez, N. Rivera, A. Fernández-González, T. Pérez, R. González, A. Hernández Battez, Electrical compatibility of transmission fluids in electric vehicles, Tribol. Int. 171 (2022), 107544, https://doi.org/10.1016/j.triboint.2022.107544.
[4] L.I. Farfan-Cabrera, A. Erdemir, J.A. Cao-Romero-Gallegos, I. Alam, S. Lee, Electrification effects on dry and lubricated sliding wear of bearing steel interfaces, Wear 516 (2023), 204592, https://doi.org/10.1016/j.wear.2022.204592.
[5] W. Ahmed Abdalglil Mustafa, F. Dassenoy, M. Sarno, A. Senatore, A review on potentials and challenges of nanolubricants as promising lubricants for electric vehicles, Lubric. Sci. 34 (2022) 1–29, https://doi.org/10.1002/ls.1568.
[6] K. Narita, D. Takekawa, Lubricants Technology Applied to Transmissions in Hybrid Electric Vehicles and Electric Vehicles, SAE Technical Paper, 2019, https://doi.org/10.4271/2019-01-2338.
[7] J. Van Rensselar, The tribology of electric vehicles, Tribol. Lubric. Technol. 75 (2019) 34–43.
[8] N. Nyholm, N. Espallargas, Functionalized carbon nanostructures as lubricant additives – a review, Carbon 201 (2023) 1200–1228, https://doi.org/10.1016/j.carbon.2022.10.035.
[9] B. Wang, F. Qiu, G.C. Barber, Q. Zou, J. Wang, S. Guo, Y. Yuan, Q. Jiang, Role of nano-sized materials as lubricant additives in friction and wear reduction: a review, Wear 490 (2022), 204206, https://doi.org/10.1016/j.wear.2021.204206.
[10] J. Zhao, Y. Huang, Y. He, Y. Shi, Nanolubricant additives: a review, Friction 9 (2021) 891–917, https://doi.org/10.1007/s40544-020-0450-8.
[11] K. Holmberg, A. Erdemir, Influence of tribology on global energy consumption, costs and emissions, Friction 5 (2017) 263–284, https://doi.org/10.1007/s40544-017-0183-5.
[12] K. Holmberg, A. Erdemir, The impact of tribology on energy use and CO_2 emission globally and in combustion engine and electric cars, Tribol. Int. 135 (2019) 389–396, https://doi.org/10.1016/j.triboint.2019.03.024.
[13] N.F. Azman, S. Samion, Dispersion stability and lubrication mechanism of nanolubricants: a review, International Journal of Precision Engineering Manufacturing-Green Technology 6 (2019) 393–414, https://doi.org/10.1007/s40684-019-00080-x.
[14] Y. Chen, P. Renner, H. Liang, Dispersion of nanoparticles in lubricating oil: a critical review, Lubricants 7 (2019) 7, https://doi.org/10.3390/lubricants7010007.
[15] R. Leslie, Rudnick. Synthetics, Mineral Oils, and BioBased Lubricants: Chemistry and Technology. Chapter 1. Polyalphaolefins, third ed., Taylor & Francis Group, LLC, 2020, 978-1-138-06821-6.
[16] A. Hernández Battez, J.F. Rico, A.N. Arias, J.V. Rodriguez, R.C. Rodriguez, J. D. Fernandez, The tribological behaviour of ZnO nanoparticles as an additive to PAO6, Wear 261 (2006) 256–263, https://doi.org/10.1016/j.wear.2005.10.001.
[17] R. Chou, A. Hernández Battez, J. Cabello, J. Viesca, A. Osorio, A. Sagastume, Tribological behavior of polyalphaolefin with the addition of nickel nanoparticles, Tribol. Int. 43 (2010) 2327–2332, https://doi.org/10.1016/j.triboint.2010.08.006.
[18] J. Viesca, A. Hernández Battez, R. González, R. Chou, J. Cabello, Antiwear properties of carbon-coated copper nanoparticles used as an additive to a polyalphaolefin, Tribol. Int. 44 (2011) 829–833, https://doi.org/10.1016/j.triboint.2011.02.006.
[19] M.K.A. Ali, H. Xianjun, R.F. Turkson, Z. Peng, X. Chen, Enhancing the thermophysical properties and tribological behaviour of engine oils using nano-lubricant additives, RSC Adv. 6 (2016) 77913–77924, https://doi.org/10.1039/C6RA10543B.
[20] R. Dubey, Y. Rajesh, M. More, Synthesis and characterization of SiO_2 nanoparticles via sol-gel method for industrial applications, Mater. Today: Proc. 2 (2015) 3575–3579, https://doi.org/10.1016/j.matpr.2015.07.098.
[21] V. Cortes, K. Sanchez, R. Gonzalez, M. Alcoutlabi, J.A. Ortega, The performance of SiO_2 and TiO_2 nanoparticles as lubricant additives in sunflower oil, Lubricants 8 (2020) 10, https://doi.org/10.3390/lubricants8010010.
[22] D.X. Peng, Y. Kang, R.M. Hwang, S.S. Shyr, Y.P. Chang, Tribological properties of diamond and SiO_2 nanoparticles added in paraffin, Tribol. Int. 42 (2009) 911–917, https://doi.org/10.1016/j.triboint.2008.12.015.
[23] D.X. Peng, C.H. Chen, Y. Kang, Y.P. Chang, S.Y. Chang, Size Effects of SiO_2 Nanoparticles as Oil Additives on Tribology of Lubricant, Industrial Lubrication and Tribology, 2010, https://doi.org/10.1108/00368791011025656.
[24] T. Sui, B. Song, Y.-h. Wen, F. Zhang, Bifunctional hairy silica nanoparticles as high-performance additives for lubricant, Sci. Rep. 6 (2016) 1–9. https://10.1038/srep22696.
[25] T. Sui, B. Song, F. Zhang, Q. Yang, Effects of functional groups on the tribological properties of hairy silica nanoparticles as an additive to polyalphaolefin, RSC Adv. 6 (2016) 393–402, https://doi.org/10.1039/C5RA22932D.
[26] N. Zawawi, W. Azmi, M. Ghazali, Tribological performance of Al_2O_3–SiO_2/PAG composite nanolubricants for application in air-conditioning compressor, Wear 492 (2022), 204238, https://doi.org/10.1016/j.wear.2022.204238.
[27] Y. Singh, E. Abd Rahim, N.K. Singh, A. Sharma, A. Singla, A. Palamanit, Friction and wear characteristics of chemically modified mahua (madhuca indica) oil based lubricant with SiO_2 nanoparticles as additives, Wear 508 (2022), 204463, https://doi.org/10.1016/j.wear.2022.204463.
[28] M. Cai, R. Guo, F. Zhou, W. Liu, Lubricating a bright future: lubrication contribution to energy saving and low carbon emission, Sci. China Technol. Sci. 56 (2013) 2888–2913, https://doi.org/10.1007/s11431-013-5403-2.
[29] I. Madanhire, C. Mbohwa, Mitigating Environmental Impact of Petroleum Lubricants, Springer, 2016, 978-3-319-31358-0.
[30] I. Otero, E.R. López, M. Reichelt, M. Villanueva, J. Salgado, J. Fernández, Ionic liquids based on phosphonium cations as neat lubricants or lubricant additives for a steel/steel contact, ACS Appl. Mater. Interfaces 6 (2014) 13115–13128, https://doi.org/10.1021/am502980m.
[31] F. Mariño, E.R. López, Á. Arnosa, M.A. González Gómez, Y. Piñeiro, J. Rivas, C. Alvarez-Lorenzo, J. Fernández, ZnO nanoparticles coated with oleic acid as additives for a polyalphaolefin lubricant, J. Mol. Liq. 348 (2022), 118401, https://doi.org/10.1016/j.molliq.2021.118401.
[32] K.I. Nasser, J.M.L. del Río, E.R. López, J. Fernández, Synergistic effects of hexagonal boron nitride nanoparticles and phosphonium ionic liquids as hybrid lubricant additives, J. Mol. Liq. 311 (2020), 113343, https://doi.org/10.1016/j.molliq.2020.113343.
[33] J.M. Liñeira del Rio, E.R. López, M. González Gómez, S. Yáñez Vilar, Y. Piñeiro, J. Rivas, D.E.P. Gonçalves, J.H.O. Seabra, J. Fernández, Tribological behavior of nanolubricants based on coated magnetic nanoparticles and trimethylolpropane trioleate base oil, Nanomaterials 10 (2020) 683, https://doi.org/10.3390/nano10040683.
[34] R. Jafari, M. Farzaneh, A simple method to create superhydrophobic aluminium surfaces, Mater. Sci. Forum 706 (2012) 2874–2879. https://doi.org/10.4028/www.scientific.net/MSF.706-709.2874.
[35] Q. Hu, H. Suzuki, H. Gao, H. Araki, W. Yang, T. Noda, High-frequency FTIR absorption of SiO_2/Si nanowires, Chem. Phys. Lett. 378 (2003) 299–304, https://doi.org/10.1016/j.cplett.2003.07.015.
[36] F. Kimura, J. Umemura, T. Takenaka, FTIR-ATR studies on Langmuir-Blodgett films of stearic acid with 1-9 monolayers, Langmuir 2 (1986) 96–101, https://doi.org/10.1021/la00067a017.
[37] E. Gadelmawla, M.M. Koura, T.M. Maksoud, I.M. Elewa, H. Soliman, Roughness parameters, J. Mater. Process. Technol. 123 (2002) 133–145, https://doi.org/10.1016/S0924-0136(02)00060-2.
[38] G. Faraci, S. Gibilisco, P. Russo, A. Pennisi, G. Compagnini, S. Battiato, R. Puglisi, S. La Rosa, Si/SiO_2 core shell clusters probed by Raman spectroscopy, Eur. Phys. J. B 46 (2005) 457–461. https://10.1140/epjb/e2005-00274-4.
[39] D.L. De Faria, S. Venâncio Silva, M. De Oliveira, Raman microspectroscopy of some iron oxides and oxyhydroxides, J. Raman Spectrosc. 28 (1997) 873–878, https://doi.org/10.1002/(SICI)1097-4555(199711)28:11<873::AID-JRS177>3.0.CO;2-B.
[40] L. Zhang, L. Chen, H. Wan, J. Chen, H. Zhou, Synthesis and tribological properties of stearic acid-modified anatase (TiO_2) nanoparticles, Tribol. Lett. 41 (2011) 409–416, https://doi.org/10.1007/s11249-010-9724-z.
[41] Z. Zachariah, P.C. Nalam, A. Ravindra, A. Raju, A. Mohanlal, K. Wang, R. V. Castillo, R.M. Espinosa-Marzal, Correlation between the adsorption and the nanotribological performance of fatty acid-based organic friction modifiers on stainless steel, Tribol. Lett. 68 (2019) 11, https://doi.org/10.1007/s11249-019-1250-z.
[42] S. Loehle, C. Matta, C. Minfray, T. Le Mogne, J.-M. Martin, R. Iovine, Y. Obara, R. Miura, A. Miyamoto, Mixed lubrication with C18 fatty acids: effect of unsaturation, Tribol. Lett. 53 (2014) 319–328, https://doi.org/10.1007/s11249-013-0270-3.
[43] R.R. Sahoo, S.K. Biswas, Frictional response of fatty acids on steel, J. Colloid Interface Sci. 333 (2009) 707–718, https://doi.org/10.1016/j.jcis.2009.01.046.

[44] B. Hamrock, D. Dowson, Minimum Film Thickness in Elliptical Contacts for Different Regimes of Fluid-Film Lubrication, Proceedings of the Society of Photo-Optical Instrumentation Engineers, 1978.
[45] D.E. Gonçalves, J.M. Liñeira del Rio, M.J.P. Comuñas, J. Fernández, J.H.O. Seabra, High pressure characterization of the viscous and volumetric behavior of three transmission oils, Ind. Eng. Chem. Res. 58 (2019) 1732–1742, https://doi.org/10.1021/acs.iecr.8b05090.
[46] H. Spikes, Mixed lubrication—an overview, Lubric. Sci. 9 (1997) 221–253, https://doi.org/10.1002/ls.3010090302.
[47] J.M. Liñeira del Rio, E.R. López, D.E. Gonçalves, J.H. Seabra, J. Fernández, Tribological properties of hexagonal boron nitride nanoparticles or graphene nanoplatelets blended with an ionic liquid as additives of an ester base oil, Lubric. Sci. 33 (2021) 269–278, https://doi.org/10.1002/ls.1543.